In-Plane 1.5 μm Distributed Feedback Lasers Selectively Grown on (001) SOI

*Ying Xue, Jie Li, Yi Wang, Ke Xu, Zengshan Xing, Kam Sing Wong, Hon Ki Tsang, and Kei May Lau**

Hetero-epitaxy for integration of efficient III-V lasers on silicon can enable wafer-scale silicon photonic integrated circuits, which can unleash the full advantages of silicon photonics in production on large silicon wafers with low cost, high throughput, and large bandwidth and large-scale integration. In this work, efficient III-V distributed feedback (DFB) lasers selectively grown on (001) silicon-on-insulator (SOI) wafers are presented. The selective hetero-epitaxy of sufficiently large areas of III-V segments allows the demonstration of DFB lasers on the SOI wafer. The fabricated DFB lasers feature a co-planar configuration with the Si layer, allowing for efficient coupling between III-V lasers and Si waveguides. The unique III-V-on-insulator structure also provides strong optical confinement for the lasers. Gratings are designed and fabricated with minimal non-radiative recombination and a simple process with good tolerance. The optically pumped DFB laser has a low lasing threshold of around 17.5 μJ cm^{-2}, stable single-mode lasing at 1.5 μm, a side-mode-suppression-ratio of over 35 dB, and a spontaneous emission factor of 0.7. The results here demonstrate a step forward towards wafer-scale integration with monolithically grown lasers, thus outlining the prospect of fully integrated Si photonics.

1. Introduction

The continuing growth of internet data traffic and the rapid increase of data traffic in data centers is driving the advance of ethernet standards to today's 400 Gb and 800 Gb s^{-1} to future standards supporting optical interconnects beyond 4 Tb/ in data centers. Photonic integration is widely recognized as the most cost-effective approach to enable the new generation of communication systems by supporting the high-capacity traffic using multiple data lanes in scalable, power-efficient, and highly compact optical transceivers. Silicon (Si) photonics, initially driven by the economics of CMOS, is the core technology for next-generation communications.[1–5] In addition, beyond the scope of communications, Si photonics is fueling various applications including imaging, sensing, spectroscopy, quantum science, and microwave engineering as a versatile platform.[6–8] Over the years, the improvement of device performance and integration complexity, especially for the passive components, have advanced the prospect of Si photonics, while further evolution has been held back by the lack of efficient monolithically integrated lasers. The main challenge lies in integrating III-V on Si in a scalable, low-cost, and process-compatible manner with the CMOS fabrication for Si photonics.[9] Heterogeneous integration, employing techniques of either wafer bonding or transfer printing, presents the most mature approach to date for the integration of III-V lasers on the Si photonics platform.[10–12] However, monolithic integration, releasing the economy of scale through direct hetero-epitaxy on large Si wafers, may offer a lower-cost alternative approach. Furthermore, petabit-per-second throughputs containing thousands of lasers with wavelength division multiplexing (WDM) and even dense wavelength division multiplexing (DWDM) require the use of monolithic integration.[13,14]

To address the challenging issue of large mismatches between III-V and Si, two mainstream methods, blanket epitaxy, and selective epitaxy have been developed for monolithic integration. For blanket epitaxy, defect engineering was realized by growing thick III-V buffer layers on Si before the stacking of laser structures.[15–17] The mitigated defect density, incorporation of quantum dots (QDs), and large design flexibility contribute to a variety of high-performance lasers on Si.[18–21] Unfortunately, the thick device and buffer layers dramatically impede efficient coupling of the lasers with other Si elements. As an alternative, selective epitaxy manipulating defects through aspect ratio trapping (ART) techniques produces III-V lasers without buffers.[22–25]

Y. Xue, J. Li, K. Xu, K. M. Lau
Department of Electronic and Computer Engineering
Hong Kong University of Science and Technology
Clear water bay, Kowloon, Hong Kong 999077, China
E-mail: eekmlau@ust.hk

Y. Wang, H. K. Tsang, K. M. Lau
Department of Electronic Engineering
The Chinese University of Hong Kong
Shatin, Hong Kong 999077, China

Z. Xing, K. S. Wong
Department of Physics and William Mong Institute of Nano Science and Technology
Hong Kong University of Science and Technology
Clear water bay, Kowloon, Hong Kong 999077, China

The ORCID identification number(s) for the author(s) of this article can be found under https://doi.org/10.1002/lpor.202300549

DOI: 10.1002/lpor.202300549

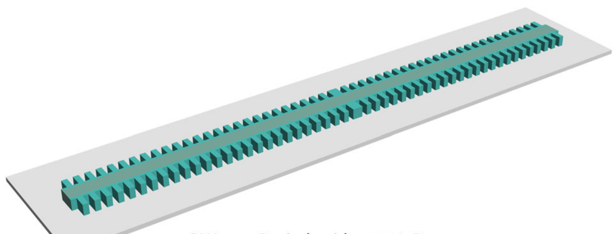

Figure 1. 3D architecture of the in-plane DFB laser on SOI.

Furthermore, selective epitaxy is essential for the goal of integrating electronics and photonics on the same chip. Nevertheless, the limited material volume at nanometer-scale generated by current selective epitaxy hinders device implementation especially electrically pumped lasers.[26,27]

Meanwhile, monolithic edge-emitting laser diodes such as distributed feedback (DFB) lasers are desirable for compact WDM sources and have been incorporated in a wide range of applications.[28–30] 1.3 μm DFB lasers on Si have been demonstrated with various grating designs using blanket epitaxy.[14,31] Impressive as the performance is, thick III-V buffers still post challenge to the fully integration, and the grating design usually involves complicated regrowth procedures or etched sidewalls leading to severe non-radiative recombination. Also, heteroepitaxy of 1.5 μm DFB lasers on Si has not been previously investigated.

In this work, we present the first 1.5 μm in-plane III-V DFB lasers selectively grown on commercial (001) SOI. Adopting the lateral aspect ratio trapping (LART) technique we developed,[32] material growth conditions were tuned to achieve high-quality and sufficiently large-area III-V on SOI for various device execution, including electrically pumped ones. Although DFB lasers with vertically stacking QWs have been widely reported, DFB lasers with laterally stacking QWs are novel and remain to be explored. We investigated the critical designs to achieve 1.5 μm lasing with lateral QWs. Unique gratings with minimized non-radiative recombination and undemanding fabrication processes were designed for the DFB lasers on SOI. Lasers with a short cavity length, low lasing thresholds, and excellent mechanical stability, exhibit stable single-mode lasing at 1.5 μm. As a result of the thin III-V-on-insulator structure, tight optical confinement in the lasers was achieved. Our demonstration here represents a highly scalable monolithic solution to integrated laser sources on Si, thus providing an elegant approach for fully integrated Si photonics with both conventional photonics and electronics.

2. Design, Materials, and Fabrication

The 3D architecture of the DFB laser on SOI is displayed in **Figure 1**. The laser features a unique III-V-on-insulator structure delivering strong optical confinement and co-planar configuration with the Si layer allowing for efficient coupling with other Si-based components. Gratings devised for the laser cavity include a quarter wave phase-shift segment placed at the center of the cavity to facilitate the single-mode lasing. Prior to experimental implementation, we theoretically evaluated the possible use of different types of gratings, as summarized in **Table 1**, including

Table 1. Comparison of various grating designs.

Grating material	Grating depth	κL	Cavity length
SiO_2	400 nm (vertical)	0.41	40 μm
SiN	400 nm (vertical)	0.94	40 μm
InP	400 nm (lateral)	2.25	40 μm

SiO_2 and SiN gratings on top of the III-V part and lateral InP gratings at sidewalls. The III-V/air surface grating was not considered here so as to allow for a low loss in the active region and easier control of the III-V dry etch. Choosing the suitable grating period and a duty cycle of 50% for these designs, the coupling strength κL was calculated to be 0.41, 0.94, and 2.25 for SiO_2 gratings, SiN gratings, and lateral InP gratings, respectively. The κL value of 2.25 is sufficient for mode selection and effective reduction of threshold gain to support single-mode lasing in a short cavity (≈40 μm). The grating depth and cavity length were set to be the same for a fair comparison. It was found that the grating depth shows little influence on the coupling strength when the depth is larger than 100 nm. Aiming for a moderate κL of around 2,[33] large flexibility on cavity length, low lasing threshold, and simplicity of fabrication process, the lateral InP grating design with the highest coupling coefficient were chosen for experimental demonstration. The grating parameters were designed with a period of 310 nm, a duty cycle of 50%, and a lateral depth of 400 nm.

Figure 2 shows the patterning processes for lateral growth and DFB laser fabrication. Starting with an 8-inch commercial (001) SOI wafer, the Si device layer was first thinned down to 480 nm by a cycled thermal oxidation at 1100 °C and oxide removal process. Then the Si layer was patterned into segments by i-line lithography and dry etch, defining the growth area of III-V, after which the Si segments were enclosed by low-temperature oxide (LTO) deposited at 600 °C.[34] Afterward, oxide openings were created at the ends of Si segments by dry etch to enable the subsequent Si undercut process. The Si undercut with a lateral depth of 8 μm was generated by wet etching in a TMAH solution to avoid etching of the oxide. As a result, parallel and smooth lateral oxide trenches with various lengths from 20 μm to 100 μm, (111) Si facet exposed at one end, were formed. Using the LART technique, the III-V materials were grown from the (111) Si facet and extended along the width guided by the lateral oxide trenches, as illustrated in cross-sectional schematics in Figure 2. After the growth of III-V materials, the LTO on top and at the sidewalls were removed by combined dry and wet etch steps to provide a clean and smooth III-V surface. Then a thin layer of plasma-enhanced chemical vapor deposited oxide was coated on the sample at 300 °C to serve as a hard mask in the following etching steps. The laser cavity with gratings was defined on the oxide hard mask and transferred to the III-V segment by E-beam lithography and one-step dry etch (Figure 2, Step 8). Finally, the end facets were polished by focused ion beam (FIB) to further reduce the mirror loss. Unlike lasers grown on Si vertically requiring partial Si removal underneath for light confinement, the DFB lasers in this work feature superior mechanical stability and better thermal dissipation as the entire III-V laser stands on the buried oxide instead of suspending. The mechanical stability has been

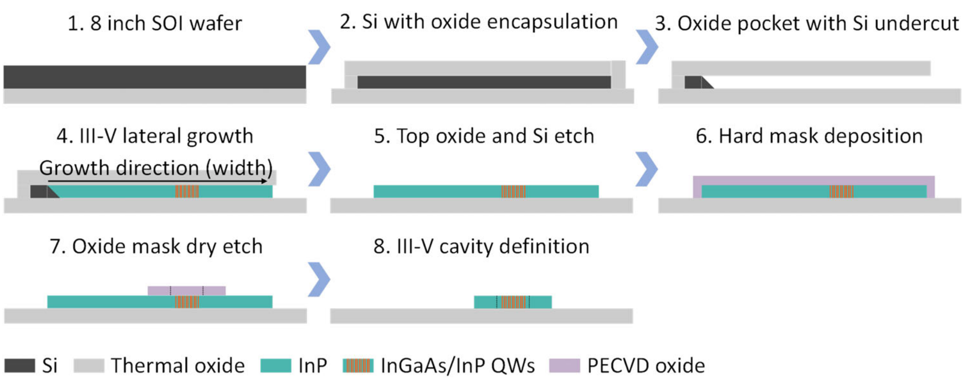

Figure 2. Fabrication process of the DFB lasers on SOI, including SOI patterning before III-V epitaxy and laser cavity formation after material growth.

proved by various processes including dry etching, wet etching, long-time sonication, high-temperature treatment, etc.

Previously, we reported the growth of high-quality III-V segments up to several micrometers long.[35] However, insufficient material volume still significantly limits the device implementation. More importantly, further extension of the material volume, especially the growth length to tens or hundreds of micrometers while maintaining high crystalline quality is fundamentally challenging due to the larger coalescence contact area and longer distance between adjacent InP nucleation islands. Here, we fine-tuned the growth of the InP nucleation layer, which determines the III-V material quality, and developed a suitable growth process to achieve high-quality and large area III-V material. By using a nucleation temperature of 385 °C, a high V/III ratio of 1400, and a growth rate of 6 nm min^{-1}, dense InP islands with small dimensions were uniformly deposited on the (111) Si facets, enabling the subsequent rapid InP coalescence process. As a result, high-quality InP segments on SOI featuring a patterned length of up to 100 µm, sufficient for various laser demonstrations, were realized. To support lasing in the telecom band, we incorporated InGaAs/InP quantum wells (QWs) as gain media, which were conformally grown on the InP with uniform morphology and high quality. The cross-sectional dark-field scanning transmission electron microscopy (STEM) image along the epitaxial direction of the as-grown III-V segment with highlighted defective Si/InP interface is displayed in **Figure 3**a. The defects were accommodated at the III-V/Si interface within a width ≈350 nm, leading to most of the III-V segments (over 6.5 µm wide) for device fabrication free of threading dislocations (TDs), antiphase boundaries (APBs), twins, and grain boundaries. The width of the III-V segments (controlled by growth time) is around 7 µm and the length (perpendicular to the epitaxial direction defined by photolithography) varied from 20 to 100 µm. They result from the smooth oxide trenches, optimal nucleation conditions, and effective defect engineering of LART. Figure 3b plotted the room temperature photoluminescence (PL) spectrum of the as-grown III-V segment with QWs inserted and pumped by a 514 nm laser diode. Figure 3c delineated the 25 periods of QWs sandwiched by the InP claddings featuring good uniformity and continuity in both directions. The superior uniformity was further verified by the zoomed-in TEM in Figure 3d. The width of the InGaAs well and InP barrier were measured to be 3 nm and 18 nm, respectively, according to the high-resolution STEM photos presented in Figure 3d,e. The atomic sharp InGaAs/InP interface along the (110) direction was presented in Figure 3e, indicating minimized non-radiative recombination via interface states. Also, the InGaAs crystal exhibits the same zinc-blende lattice pattern as InP. The InGaAs/InP QWs were further investigated by energy-dispersive X-ray spectroscopy as revealed by the elemental mapping in Figure 3f. The detected signal of each element generates a clear contrast at the InGaAs/InP interfaces without element mixing, confirming the sharp transition between InP and InGaAs. The indium composition was found to be around 60%, suggesting compressively strained InGaAs quantum wells. No relaxation was found with the thin InGaAs well, in good agreement with the clean InGaAs/InP interfaces without defects. The quality of III-V segments was also evaluated by multiple TEM lamellae prepared perpendicular to the epitaxial direction including the MQW sections and InP sections. Limited by the maximum dimension of ≈10 µm for the TEM lamellae can be prepared, we prepared TEM lamellae on various segments and different positions on the same segment to verify the crystalline quality of the III-V crystals. The STEM images in both dark field, bright field, and various magnifications are presented in Figure 3g including 1) BF-STEM of MQW section, 2) BF-STEM of MQW section, 3) DF-STEM of MQW section, 4) DF-STEM of InP section, and 5) DF-STEM of InP section, which confirmed the TD, APB, twin, and grain boundary free feature.

The scanning electron microscopy (SEM) image in **Figure 4**a illustrates the finished DFB laser on SOI. The adjacent DFB laser and III-V segment without fabrication are also included. The fabricated DFB lasers feature a width of 1.9 µm (including the 400 nm wide lateral gratings) and a length of 40 µm or 80 µm. A $\lambda/4$ phase shift was fabricated in the center of the cavity to enable single-mode lasing, as depicted in the top-view optical image in Figure 4b. The straight end facet of the as-grown III-V segments can be figured out by the outline of the oxide underneath, generated during the oxide etching process (Steps 5 and 7 in Figure 2). The gratings with a period of 310 nm and a duty cycle of 50% demonstrate smooth and vertical sidewalls, as confirmed by the tilted-view SEM image in Figure 4c. The over-etch of oxide was caused by the oxide removal step after the fabrication. Figure 4d exhibits the mirror-like end facet of the DFB laser after the FIB polishing. The dimensions of the gratings agree well with the design and demonstrate satisfactory uniformity, as evidenced in Figure 4e. In this laser design, although QWs with a larger

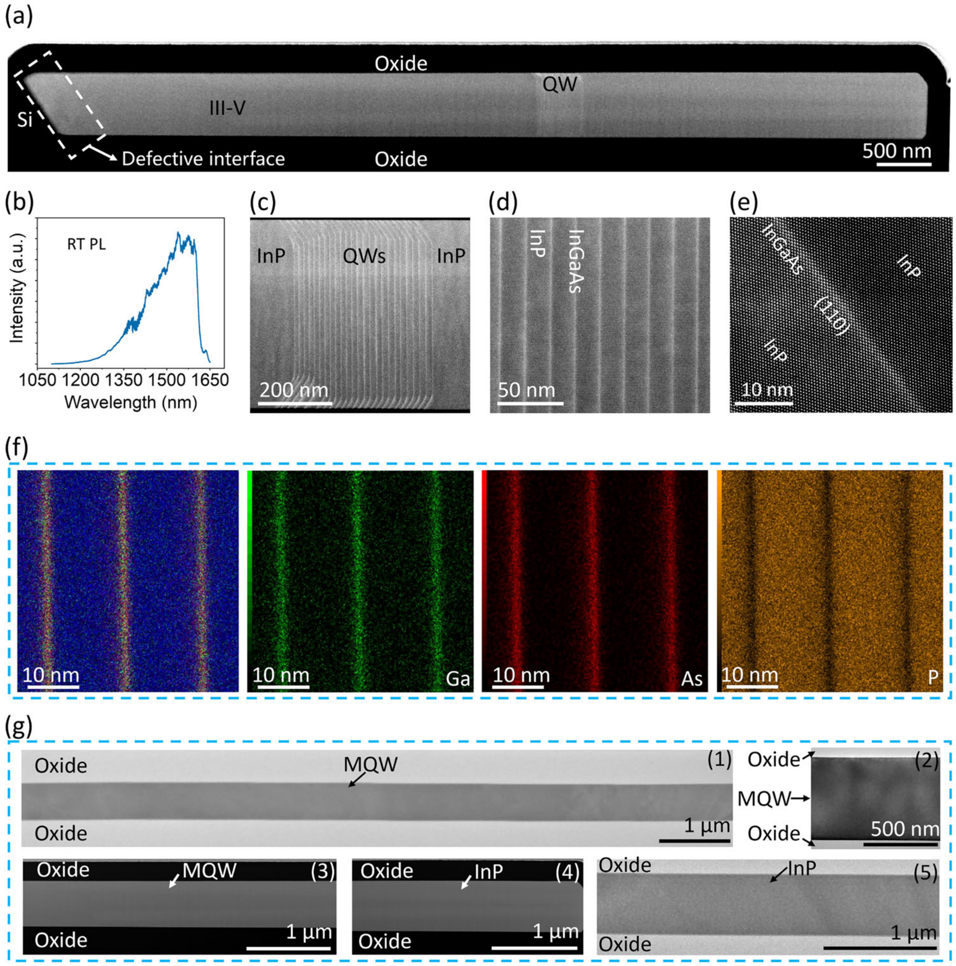

Figure 3. a) Global-view STEM image along growth direction illustrating the cross-section of the entire as-grown III-V segment. b) Room temperature (RT) PL of the as-grown III-V segment with QWs. c) 25 period ofInGaAs/InP QWs sandwiched by the InP claddings. d) Zoomed-in STEM image showing the uniformity of the QWs. e) STEM image of the atomic sharp InGaAs/InP interface. f) Color-overlaid elemental mapping of all the elements, Gallium in green, Arsenic in red, and Phosphorus in orange. g) STEM images of multiple TEM lamellae prepared at various segments perpendicular to growth direction: 1) BF-STEM of MQW section; 2) BF-STEM of MQW section; 3) DF-STEM of MQW section; 4) DF-STEM of InP section; 5) DF-STEM of InP section.

carrier diffusion length compared with QDs were adopted, non-radiative recombination could be minimized. The III-V/oxide interfaces (previously Si/oxide interfaces) in the device region, serving as the sidewalls of vertically oriented QWs, are dislocation-free because of the ART technique. Etching processes serve as the sidewalls of the laser cavity only. Furthermore, the gratings were defined with the cavity simultaneously in one-step etching, realizing a simplified fabrication process and a robust integration method with less uncertainties. Prior to the demonstration of telecom DFB lasers, 950 nm bulk InP Fabry-Perot (FP) lasers on SOI with a width of 1 µm and a length of 40 µm were fabricated for evaluation of the lateral grown InP as light sources in Si photonics. We grew InP without QWs insertion using LART on the same SOI platform and fabricate InP FP lasers along the length of the InP segment following similar steps as the fabrication of 1.5 µm DFB lasers on SOI. The finished 950 nm bulk InP FP laser with polished end facets was displayed in the tilted-view SEM image in the inset of **Figure 5**b.

3. Results and Analysis

The fabricated lasers were characterized in a micro-photoluminescence (µ-PL) system, which used a mode-locked Ti/sapphire laser, emitting 750 nm center wavelength pulses of about 100 fs pulse width at a repetition rate of 76 MHz for pumping the DFB laser, and a thermo-electric-cooled InGaAs detector for detecting the PL. A cylindrical lens was placed in the incident optical beam to convert the round spot from the excitation laser to a line-shaped illumination focused to a size of ≈55 µm × 1.5 µm. The bulk InP Fabry–Perot (FP) lasers were first measured, and the results are shown in Figure 5. The emission spectra below and above the lasing threshold are plotted in Figure 5a. With the increase of pumping power, the broad envelope of spontaneous emission became narrower to form the multimode lasing spectrum, with modes at around 950 nm stood out. The light–light (L–L) curve was extracted from the power-dependent spectrum and displayed in Figure 5b, showing

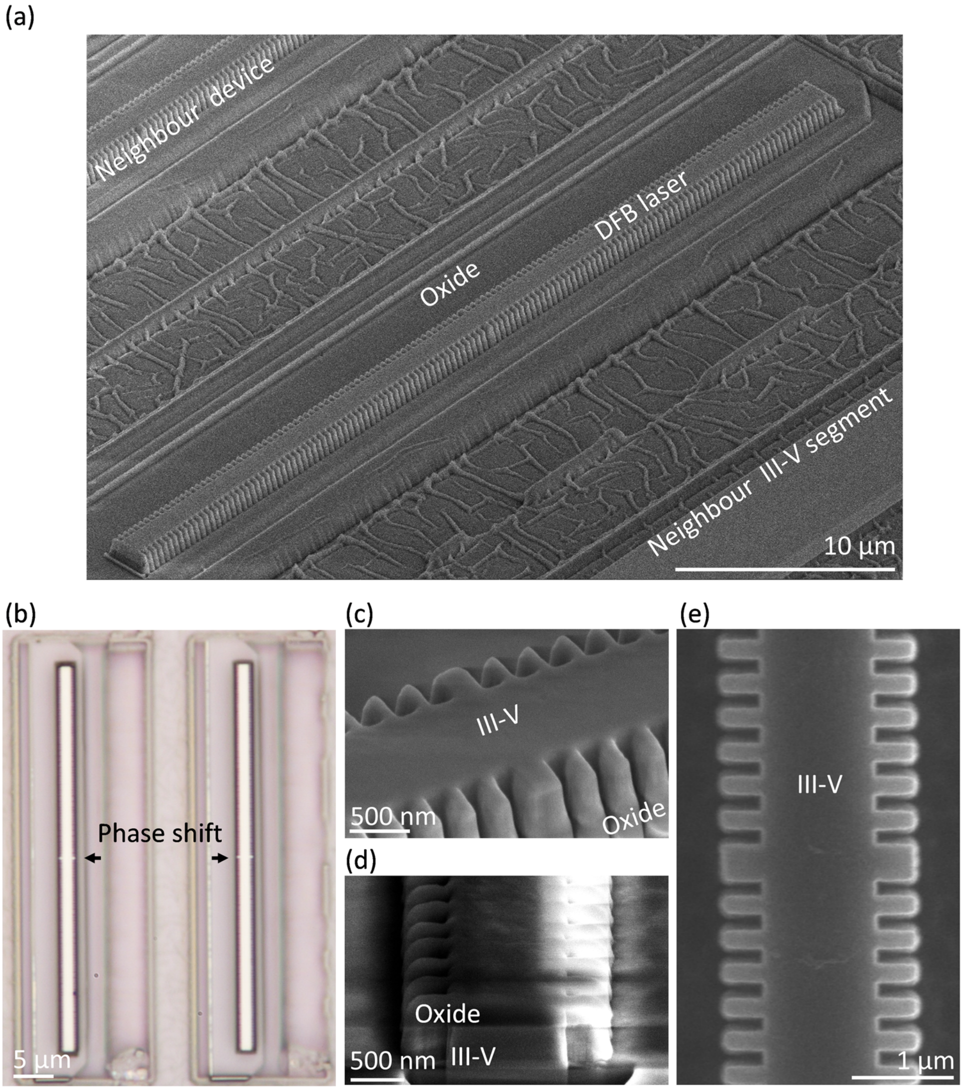

Figure 4. a) Tilted view SEM image of the finished DFB lasers and adjacent III-V segment on SOI. b) Optical image of the DFB lasers on SOI. c) SEM image showing the details of the gratings. d) SEM image of the end facet of the DFB laser on SOI. e) Top view SEM image presenting the uniformity of the lateral gratings.

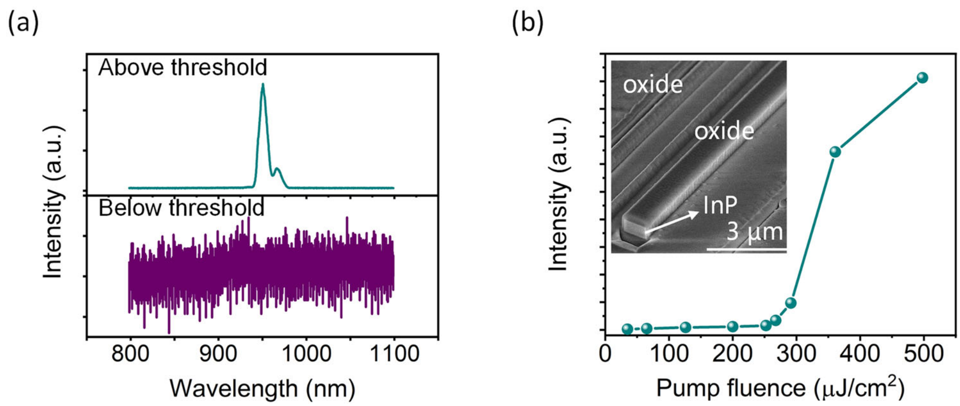

Figure 5. a) Room temperature lasing spectrum below and above the threshold of the bulk InP FP laser on SOI. b) Extracted *L–L* curve of the bulk InP FP lasers on SOI; inset: SEM image of the finished InP FP laser on SOI.

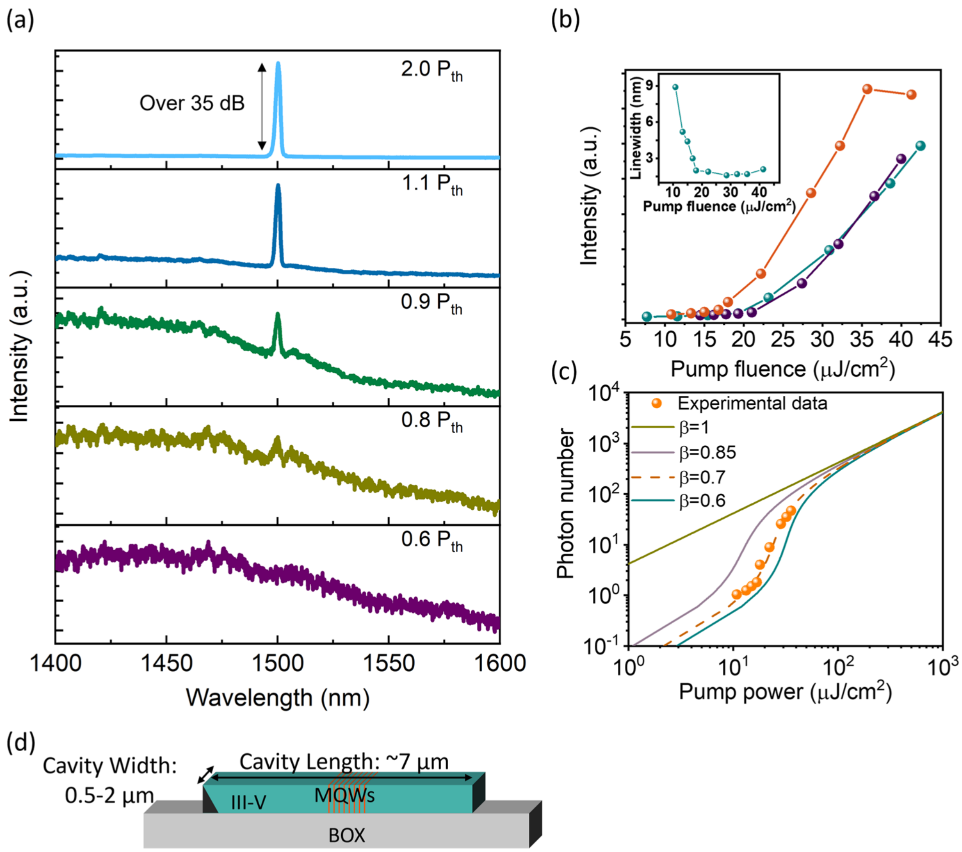

Figure 6. a) Room temperature spectra of the DFB laser on SOI at various pumping powers. b) Measured *L–L* curves of the DFB lasers on SOI; inset: linewidth evolution proving the lasing behavior. c) Rate equation model solutions for various β values with β of 0.7 delivers the best fit to the experimental data. d) Laser cavity along epitaxial direction.

an extrapolated lasing threshold of 270 µJ cm^{-2}. A spontaneous emission factor β of 0.25 was derived by fitting the experimental data. With the extended epitaxial InP, we can fabricate FP lasers resonating perpendicular to the growth direction, excluding the Si and defective Si/III-V interface. Compared with the InP FP lasers resonating along the growth direction reported in,[32] we obtained comparable thresholds and a 100 times higher output power using the same measurement setup, despite the cavity volume being about 27 times larger. The fabricated lasers demonstrated a high lasing yield of over 90%, which indicated the high quality of the epitaxial InP in this large volume.

The DFB lasers with QWs on SOI were characterized using the same µ-PL system with a different dichroic mirror. Due to the limitation of the focused cylindrical lens spot size, we only characterized DFB lasers with 40 µm cavity length. The room temperature emission spectrum of the DFB lasers on SOI at various pumping power is shown in **Figure 6**a. Below the threshold, we measured a broad spontaneous emission spectrum. With increasing pump power, spectral narrowing with a peak at 1.5 µm wavelength dominated the spectrum, and the device operated as a DFB laser. Stable laser operation was demonstrated with all the lasers measured, and they all operated at a lasing wavelength of 1.5 µm, as defined by the DFB grating period. A side-mode-suppression-ratio (SMSR) exceeding 35 dB was measured, and the measurement might be limited by the method of light collection. Figure 6b presents representative *L-L* curves in linear scale measured from the DFB lasers on SOI with the same grating design. The DFB lasers manifest low thresholds, with the lowest one around 17.5 µJ cm^{-2}, 10 times lower than those of reported nano-lasers.[36] The rolloff at high pump power is caused by the accumulated heat from excitation as our lasers were tested on the stage without heat dissipation or temperature controller. Note that the DFB lasers can also lase with etched end facets without FIB polishing. The measured linewidth as a function of pump fluence is plotted in the inset of Figure 6b. The linewidth was limited by the pulsed pumping, which introduced a time-dependent free carrier density in the cavity and produced frequency chirp in the output of the laser.[37] The spontaneous emission factor β, determining the threshold and linewidth, was calculated based on the rate equation model. By fitting the experimental data with the theoretical model, we can obtain a high β value of 0.7 for the DFB laser, as shown in Figure 6c. While DFB lasers generally require a long cavity over 100 µm length, our DFB lasers on SOI demonstrate superior lasing performance with a short cavity length of 40 µm, suggesting high quality of the selectively grown epitaxial III-V on SOI platform and high efficiency of the cavity design. Compared with the bulk InP lasers with smaller cavity volume and pumped by the same laser at 750 nm wavelength, we observed a 94% threshold reduction with the DFB QW lasers and a significant linewidth shrinkage. The ratio of the InP laser

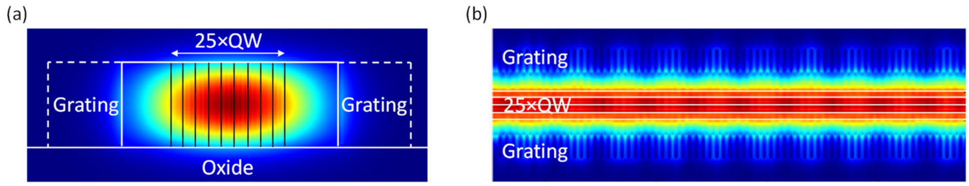

Figure 7. a) Cross-sectional optical mode profile of fundamental mode inside the DFB laser. b) Field plot of the mode (normalized to the end facet of cavity) in the DFB laser on SOI.

threshold over QW laser threshold in this work is around two times the ratio we observed previously between the InP FP lasers and QW FP lasers grown by vertical ART. These improvements can be attributed to the following reasons: 1) The smaller gain volume and stronger carrier confinement of QWs. 2) The higher optical feedback efficiency of the fabricated gratings. (3) The grating does not introduce significant non-radiative recombination. We also fabricated QW lasers along the epitaxial direction with a cavity length of ≈7 μm and cavity widths of 0.5, 1, and 2 μm as illustrated in Figure 6d but didn't observe lasing, which further suggests the strong effect of non-radiative recombination reduction by excluding the defective Si/InP interface. Compared with other reported works, our lasers present superior overall performance in terms of lasing wavelength, threshold, spontaneous emission factor, optical confinement, and SMSR.[22,23,32,36–38]

To study the lasing behavior, we performed finite-difference-time-domain simulations. The fundamental mode was estimated to be the lasing mode due to the largest confinement factor, highest reflectivity, and good agreement with the experimental result. From the perspective of integration with the passive components, the fundamental mode is preferred as the higher-order modes may encounter larger scattering loss, and tapers may introduce further loss.[39] **Figure 7**a plots the field distribution of the mode inside the DFB laser showing the strong in-plane feedback provided by the gratings. The cross-sectional optical mode profile of the fundamental mode is depicted in Figure 7b. The confinement factor in the QWs was calculated to be as high as 17.6%, which benefited from the tight optical confinement of the QWs and the unique III-V-on-insulator structure. The high confinement factor and small thickness of the III-V lasers working well with the short laser cavity design may enable a fast direct modulation speed.[40,41]

4. Conclusion and Outlook

The next major challenge is the fabrication of electrically pumped lasers. We believe a possible way to achieve this is to grow p-InGaAs and n-InP contact layers, and fabrication of distributed feedback gratings or distributed Bragg reflectors. To improve carrier and optical confinement, quaternary compounds such as InAlGaAs might need to be incorporated. Although the III-V material length has been extended to 100 μm, lower contact resistance, and mirror loss can help support lasing without generating excessive heat or loss. Longer III-V segment around 500 μm will further benefit the lasing.[27] Also, designs to provide low metal-induced loss are essential for the lasing. Based on our previous work of Si-waveguide coupled III-V photodetectors with coupling efficiency of over 75%, the light can be potentially coupled from lasers to Si waveguides in a butt-coupling scheme with high efficiency.[42] Tapers can be involved to improve the coupling efficiency and structures such as sub-wavelength gratings can be applied to further reduce reflections. Electrically pumped lasers can also be achieved by selective regrowth of the active region on top of the III-V segments, in which case the quantum dots with stronger confinement can be applied.

In conclusion, we have reported the fabrication of efficient III-V DFB lasers selectively grown on commercial (001) SOI and we demonstrated a highly scalable monolithic solution for integrated laser sources on Si. The DFB lasers on SOI feature a coplanar design, with the III-V active region at the same level as silicon waveguides, facilitating efficient coupling between the III-V lasers and passive silicon waveguide components in future designs. The optical structure of the III-V-on-insulator provides excellent optical confinement, with a confinement factor of 17.6%. Our work showed minimal non-radiative recombination, and we demonstrated that the gratings can be made in a simple fabrication process, offering excellent mechanical stability and is suitable for use in DFB lasers on SOI. The DFB QW laser demonstrates a low lasing threshold of around 17.5 μJ cm^{-2}, lasing wavelength of 1.5 μm, large spontaneous emission factor of 0.7, and SMSR exceeding 35 dB. Furthermore, the large-area III-V segments used in this work can provide sufficient volume and laser quality for the demonstration of electrically pumped lasers in the future. The work presented here provides a novel solution of on-chip lasers for PIC and outlines the prospect of fully integrated Si photonics.

Acknowledgements

Y.X. and J.L. contributed equally to this work. This work was supported by the Research Grants Council, University Grants Committee (16213420), and the Innovation and Technology Fund (ITS/226/21FP). The authors would like to thank the Nanosystem Fabrication Facility (NFF) and Material Characterization & Preparation Facility (MCPF) of HKUST for their technical support.

Conflict of Interest

The authors declare no conflict of interest.

Data Availability Statement

The data that support the findings of this study are available from the corresponding author upon reasonable request.

Keywords

DFB laser, monolithic integration, silicon photonics

Received: June 15, 2023
Revised: July 10, 2023
Published online:

[1] M. Near, C. Xiang, S. M. Bowers, A. Bjorlin, R. Blum, E. Bowers, *Appl. Phys. Lett.* **2021**, *118*, 220501.
[2] D. Thomson, A. Zilkie, J. E. Bowers, T. Komljenovic, G. T. Reed, L. Vivien, D. Marris-Morini, E. Cassan, L. Virot, J.-M. Fédéli, J. Hartmann, J. H. Schmid, D. Xu, F. Boeuf, P. O'Brien, G. Z. Mashanovich, M. Nedeljkovic, *J. Opt.* **2016**, *18*, 073003.
[3] D. Liang, J. E. Bowers, *Nat. Photonics* **2010**, *4*, 511.
[4] A. Y. Liu, J. E. Bowers, *IEEE J. Sel. Top. Quantum Electron.* **2018**, *24*, 6000412.
[5] G. Roelkens, L. Liu, D. Liang, R. Jones, A. Fang, B. Koch, J. Bowers, *Laser Photonics Rev.* **2010**, *4*, 751.
[6] A. Z. Subramanian, E. Ryckeboer, A. Dhakal, F. Peyskens, A. Malik, B. Kuyken, H. Zhao, S. Pathak, A. Ruocco, A. De Groote, P. Wuytens, D. Martens, F. Leo, W. Xie, U. D. Dave, M. Muneeb, P. Van Dorpe, J. Van Campenhout, W. Bogaerts, P. Bienstman, N. L. Thomas, D. Van Thourhout, Z. Hens, G. Roelkens, R. Baets, *Photonics Res.* **2015**, *3*, B47.
[7] Z. Zhang, Y. Li, Y. Wang, Z. Yu, X. Sun, H. K. Tsang, *Laser Photonics Rev.* **2021**, *15*, 2100039.
[8] M. Hermans, M. Burm, T. V. Vaerenbergh, J. Dambre, P. Bienstman, *Nat. Commun.* **2015**, *6*, 6729.
[9] Y. Han, H. Park, J. Bowers, K. M. Lau, *Adv. Opt. Photonics* **2022**, *14*, 404.
[10] Y. Wan, C. Xiang, J. Guo, K. Roscica, M. J. Kennedy, J. Selvidge, Z. Zhang, L. Chang, W. Xie, D. Huang, A. C. Gossard, *Laser Photonics Rev.* **2021**, *15*, 2100057.
[11] J. Zhang, G. Muliuk, J. Juvert, S. Kumari, J. Goyvaerts, B. Haq, C. Op de Beeck, B. Kuyken, G. Morthier, D. Van Thourhout, R. Baets, G. Lepage, P. Verheyen, J. Van Campenhout, A. Gocalinska, J. O'Callaghan, E. Pelucchi, K. Thomas, B. Corbett, A. J. Trindade, G. Roelkens, *APL Photonics* **2019**, *4*, 110803.
[12] Z. Zhou, B. Yin, J. Michel, *Light: Sci. Appl.* **2015**, *4*, e358.
[13] J. Liu, J. Zhang, J. Liu, Z. Lin, Z. Li, Z. Lin, J. Zhang, C. Huang, S. Mo, L. Shen, S. Lin, Y. Chen, R. Gao, L. Zhang, X. Lan, X. Cai, Z. Li, S. Yu, *Light: Sci. Appl.* **2022**, *11*, 202.
[14] Y. Wan, J. C. Norman, Y. Tong, M. J. Kennedy, W. He, J. Selvidge, C. Shang, M. Dumont, A. Malik, H. K. Tsang, A. C. Gossard, J. E. Bowers, *Laser Photonics Rev.* **2020**, *14*, 2000037.
[15] W. Luo, Y. Xue, J. Huang, L. Lin, B. Shi, K. M. Lau, *Photonics Res.* **2020**, *8*, 1888.
[16] S. Zhu, B. Shi, Q. Li, K. M. Lau, *Opt. Express* **2018**, *26*, 14514.
[17] S. Chen, W. Li, J. Wu, Q. Jiang, M. Tang, S. Shutts, S. N. Elliott, A. Sobiesierski, A. J. Seeds, I. Ross, P. M. Smowton, H. Liu, *Nat. Photonics* **2016**, *10*, 307.
[18] Y. Xue, W. Luo, S. Zhu, L. Lin, B. Shi, K. M. Lau, *Opt. Express* **2020**, *28*, 18172.
[19] Y. Wan, S. Zhang, J. C. Norman, M. J. Kennedy, W. He, Y. Tong, C. Shang, J. J. He, H. K. Tsang, A. C. Gossard, J. E. Bowers, *Laser Photonics Rev.* **2020**, *14*, 1900348.
[20] T. Zhou, M. Tang, G. Xiang, B. Xiang, S. Hark, M. Martin, T. Baron, S. Pan, Z. L. Park, S. Chen, Z. Zhang, H. Liu, *Nat. Commun.* **2020**, *11*, 977.
[21] C. Shang, E. Hughes, Y. Wan, M. Dumont, R. Koscica, J. Selvidge, R. Herrick, A. C. Gossard, K. Mukherjee, J. E. Bowers, *Optica* **2021**, *8*, 749.
[22] Y. Han, Z. Yan, W. K. Ng, Y. Xue, K. S. Wong, K. M. Lau, *Optica* **2020**, *7*, 148.
[23] Y. Shi, Z. Wang, J. Van Campenhout, M. Pantouvaki, W. Guo, B. Kunert, D. Van Thourhout, *Optica* **2017**, *4*, 1468.
[24] W. Stephan, B. F. Mayer, H. Schmid, M. Sousa, J. Gooth, H. Riel, E. Moselund, *ACS Nano* **2018**, *12*, 2169.
[25] Y. Han, Z. Yan, Y. Xue, K. M. Lau, *Appl. Phys. Lett.* **2020**, *117*, 052102.
[26] M. B. Schmid, K. L. G. Moselund, C. M. J. B. Breslin, D. Cutaia, H. Riel, *Appl. Phys. Lett.* **2015**, *106*, 233101.
[27] Y. Han, Y. Xue, Z. Yan, K. M. Lau, *J. Lightware Technol.* **2021**, *39*, 940.
[28] Z. Yang, Z. Ding, L. Liu, H. Zhong, S. Cao, X. Zhang, S. Lin, X. Huang, H. Deng, Y. Yu, S. Yu, *Photonics Res.* **2022**, *10*, 1271.
[29] J. Rahimi, J. Van Kerrebrouck, B. Haq, J. Bauwelinck, G. Roelkens, G. Morthier, *IEEE J. Sel. Top. Quantum Electron.* **2021**, *28*, 1.
[30] Z. Wang, A. Abbasi, U. Dave, A. De Groote, S. Kumari, B. Kunert, C. Merckling, M. Pantouvaki, Y. Shi, B. Tian, K. Van Gasse, *Laser Photonics Rev.* **2017**, *11*, 1700063.
[31] Y. Wang, S. Chen, Y. Yu, L. Zhou, L. Liu, C. Yang, M. Liao, M. Tang, Z. Liu, J. Wu, W. Li, I. Ross, A. J. Seeds, H. Liu, S. Yu, *Optica* **2018**, *5*, 528.
[32] Z. Yan, Y. Han, L. Lin, Y. Xue, C. Ma, W. K. Ng, K. S. Wong, K. M. Lau, *Light: Sci. Appl.* **2021**, *10*, 200.
[33] J. E. Whiteaway, G. H. B. Thompson, A. J. Collar, C. J. Armistead, *IEEE J. Quantum Electron.* **1989**, *25*, 1261.
[34] Y. Xue, Y. Han, Y. Tong, Z. Yan, Y. Wang, Z. Zhang, H. K. Tsang, K. M. Lau, *Optica* **2021**, *8*, 1204.
[35] J. Li, Y. Xue, L. Lin, Z. Xing, K. S. Wong, K. M. Lau, *J. Light. Technol.* **2022**, *40*, 5631.
[36] H. Kim, W. J. Lee, T. Y. Chang, D. L. Huffaker, *Phys. Status Solidi Rapid Res. Lett.* **2019**, *13*, 1800489.
[37] Z. Wang, B. Tian, M. Pantouvaki, W. Guo, P. Absil, J. Van Campenhout, C. Merckling, D. Van Thourhout, *Nat. Photonics* **2015**, *9*, 837.
[38] B. Tian, Z. Wang, M. Pantouvaki, P. Absil, J. Van Campenhout, C. Merckling, D. Van Thourhout, *Nano Lett.* **2017**, *17*, 559.
[39] S. Uvin, S. Kumari, A. De Groote, S. Verstuyft, G. Lepage, P. Verheyen, J. Van Campenhout, G. Morthier, D. Van Thourhout, G. Roelkens, *Opt. Express* **2018**, *26*, 18302.
[40] H. Altug, D. Englund, J. Vuckovic, *Nat. Phys.* **2006**, *2*, 484.
[41] S. Yamaoka, N. P. Diamantopoulos, H. Nishi, R. Nakao, T. Fujii, K. Takeda, T. Hiraki, T. Tsurugaya, S. Kanazawa, H. Tanobe, T. Kakitsuka, *Nat. Photonics* **2021**, *15*, 28.
[42] Y. Xue, Y. Han, Y. Wang, J. Li, J. Wang, Z. Zhang, X. Cai, H. K. Tsang, K. M. Lau, *Optica* **2022**, *9*, 1219.